Optimizing Energy Consumption for Lighting Control System via Multivariate Extremum Seeking Control With Diminishing Dither Signal

Chun Yin, *Member, IEEE*, Sara Dadras, *Senior Member, IEEE*, Xuegang Huang, YangQuan Chen, *Senior Member, IEEE*, and Shouming Zhong

***Abstract*— Because that the light-energy consumption (LC) is growing quite dramatically over the past decades, the light-energy efficiency is regarded as a key component of the modern energy system in major cities. In this paper, a novel and sophisticated algorism of lighting control is presented to improve light-energy efficiency and cut down energy consumption, when considering the lighting system with multilighting equipment. In this paper, a multivariate extremum seeking controller is used to manipulate, respectively, the luminance of multilighting equipment, in order to track the minimal LC efficiently. Meanwhile, a proportional–integral–differential (PID) approach is adopted to achieve the required level of illumination. The proposed extremum seeking control (ESC) is designed to ensure the amplitude of the dither signal converge exponentially to zero, by making the amplitudes change with the extremum estimation error. The presented frame helps to improve search speed for the minimal LC value and remove the steady-state oscillations. The comparative experiments reveal that, compared with the convergence velocity of the Newton- and gradient-based ESCs, the developed method for the track of the minimal LC can have higher accuracy and faster speed.**

***Note to Practitioners*—In a modern large commercial building, the exorbitant LC is an important problem for the engineering technicians and managers, and the hybrid lighting system which combines artificial light with natural light offers a solution to this problem. However, the minimum light-energy optimal control is a very key problem in manipulating multigroup lighting equipment, since the required level of illumination usually varies according to the exterior lighting environment. This paper contributes to a useful multivariate extremum seeking controller to solve these light-energy control problems for multiple-input single-output hybrid lighting system, whereas the PID controller is also designed to maintain the required level of illumination simultaneously. This paper discusses how to seek the minimal energy necessary for the required levels of illumination by separately regulating different light equipment. The research results of this paper will be beneficial for a practical application of extremum seeking control method in enhancing the lighting energy efficiency of lighting system.**

***Index Terms*— Diminishing dither signal, light-energy consumption (LC), lighting control, multivariate extremum seeking control.**

I. Introduction

AT THE present time, the search for the promising solutions of energy problems has increasingly attracted much attentions around economic and industrial society. Moreover, there have been escalating attentions toward the enhancement of energy efficiency (see [1]–[4]). Currently, light-energy consumption (LC) is a major division of the building energy consumption, especially for some large commercial buildings (i.e., airport, hotel, office town, school, supermarket, railway station, etc.) [5], [6]. As reported from the U.S. Department of Energy, the 14% of the whole electric consumption in business buildings was attributable to the lighting consumption [7]. Recently, various types of techniques are attempted to reduce the lighting electric energy while realizing optimal lighting environments (see [8]–[12]), such as electricity saving lamp, energy harvesting system, optimizing control strategy, and efficient distribution design. Hybrid lighting is thought to be an environmentally friendly and energy conservation method to cut down the lighting electric energy by combining natural and artificial light efficiently [13]. Because that the external nature lighting circumstances are always varying, the adjustment of artificial light can guarantee the actualization of the required level of illumination. Meanwhile, there should be a real-time optimal technique to realize the track of the minimal LC of artificial lighting by regulating multilighting equipment. Thus, the track of the minimal LC can be deemed to be the extremum seeking control (ESC) situation.

Manuscript received May 1, 2018; revised October 29, 2018 and February 8, 2019; accepted February 19, 2019. Date of publication March 13, 2019; date of current version October 4, 2019. This paper was recommended for publication by Associate Editor Q. Zhao and Editor J. Li upon evaluation of the reviewers' comments. This work was supported by National Basic Research Program of China (Grant No.61873305, 61503064 and 51502338), and Sichuan Science and Technology Plan Project (Grant 2018JY0410 and 2019YJ0199). *(Corresponding authors: Chun Yin; Xuegang Huang.)*

C. Yin is with the School of Automation Engineering, University of Electronic Science and Technology of China, Chengdu 611731, China (e-mail: yinchun.86416@163.com).

S. Dadras is with the Electrical and Computer Engineering Department, Utah State University, Logan, UT 84321 USA (e-mail: s_dadras@ieee.org).

X. Huang is with the Hypervelocity Aerodynamics Institute, China Aerodynamics Research and Development Center, Mianyang 621000, China (e-mail: emei-126@126.com).

Y. Chen is with the Mechatronics, Embedded Systems and Automation Laboratory, School of Engineering, University of California at Merced, Merced, CA 95343 USA (e-mail: ychen53@ucmerced.edu).

S. Zhong is with the School of Mathematics Sciences, University of Electronic Science and Technology of China, Chengdu 611731, China.

Color versions of one or more of the figures in this article are available online at http://ieeexplore.ieee.org.

Digital Object Identifier 10.1109/TASE.2019.2901432

ESC as a famous real-time optimal algorithm has a high probability of realizing the track of a varying optimal point by regulating the control input (see [14]–[19]). Ashley and Andersson [20] applied ESC for 3-D diffusing sources. In previous research studies, sliding-mode-based ESC (SM-ESC) in [21] and [22] was implemented to maximize the electric energy saving of two-group lighting equipment. However, the ESCs mentioned earlier were just employed in the single-input single-output (SISO) environments. Furthermore, it should be noted that they could not be implemented in the investigation of the general hybrid lighting involving multilighting equipment. Therefore, it is necessary to develop a multivariate ESC to realize the minimal LC tracking for multilighting equipment, when maintaining the required level of illumination. On the other hand, it should be emphasized that there exist few investigations and research studies (see [23]–[26]) of extremum seeking framing for multiinputs circumstances. Moreover, there are also few reports about multivariate ESCs applications for multilighting equipment. Both of Newton- and gradient-based ESCs can be thought as the feasible methods for minimal LC tracking problems of multilighting equipment. In [27], the Newton method was applied for Multi-input Single output (MISO) lighting systems. Yin *et al.* [28] adopted the fractional-order (FO) gradient-based ESC to realize the track of minimal LC. However, the methods mentioned earlier (see [27] and [28]) have a possibility to bring about the unwelcome oscillations due to the changeless amplitudes of the dither signal, since that these amplitudes are the primary parameters that determine both oscillations and track efficiency. In addition, they could cause inferior performance in real applications. This requires a tradeoff between oscillations and track efficiency. Hence, it is important to improve the control performance of multivariate ESC. It also needs to propose an enhanced multivariate ESC for lighting systems involving multilighting equipment, to not only realize the track of the minimal LC but also promote the seeking efficiency.

In this paper, a real-time optimal control strategy, including a novel multivariate ESC, is developed for hybrid lighting with multilighting equipment, to enhance energy-saving efficiency. The multivariate ESC with diminishing dither signal is designed to enhance the search rate and get rid of the steady-state oscillations, to guarantee effectively the minimal LC tracking. The proposed ESC can also guarantee the amplitudes of the dither signal exponentially converge to zero, by making the amplitudes vary with the extremum estimation error. Experiment results verify that the designed ESC is better than the corresponding Newton- and gradient-based ESCs while realizing the required level of illumination via proportional–integral–differential (PID).

II. Lighting System

A. Problem Formulation

Hybrid lighting can be deemed to be an effective energy-conservation and lower cost lighting technology which unites natural light and artificial light efficiently. It attributes a lot to energy-saving and delightful interior light-environments

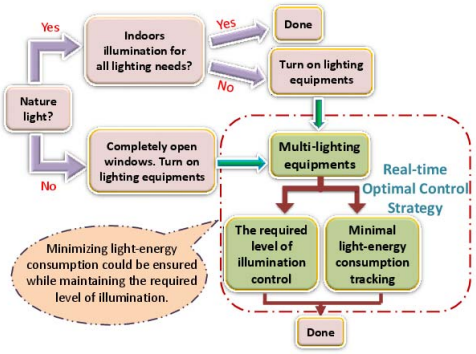

Fig. 1. Real-time optimal control strategy schematic.

of architectures. Considering the changing external nature lighting circumstances, the hybrid lighting system can maintain the appropriate interior lighting condition by adjusting multilighting equipment, according to the illumination signal from photometric sensor. However, at the same time, it is obvious that LC in the hybrid lighting system could be further reduced through the dynamic regulation of the groups of artificial lighting equipment.

That is, manipulating the groups of lighting equipment can maintain the required level of illumination, but LC will be changed accordingly for various energy allocation. Hence, as shown in Fig. 1, a real-time optimal control algorithm is designed to reduce unnecessary electric energy consumption and improve illumination efficiency while maintaining the appropriate interior lighting condition.

B. System Description

To illustrate the above-mentioned detail, a minihouse based on Arduino module is built like the following: the programmable prototyping platform of Arduino2560 is applied as a center component of this minihouse, which serves as the data-gathering board for MATLAB/Simulink with the help of Instrument Control Toolbox. The size of the minihouse is measured as 60 cm in length, 40 cm in width, and 90 cm in height, in which the storey height is 30 cm. Next, the lighting experiments were conducted on the ground floor of minihouse. As depicted in Fig. 2, the ground floor includes 11 LEDs and a GY-30 light sensor. I^2C bus interface helps bringing out the connection between GY-30 light sensor and Arduino2560. In order to further demonstrates how the proposed system works, the 11 LEDs on the ceiling were cut into n groups. It should be mentioned that there are 15 pulsewidth modulation (PWM) ports offered 8-bits PWM output in Arduino2560. Subsequently, the luminance of each-group LEDs can be operated by the PWM signal. That is to say, each-group luminance can be manipulated via the corresponding PWM signal's duty cycle.

Remark 1: The experiment applies the PWM output signal to the minihouse's current input, to adjust the luminance of n group lighting equipment. We send the control value υ in the Simulink model to Arduino2560 through the PWM output ports. Since the PWM ports in Arduino2560 are 8-bits PWM output, the range of υ is required from 0 to 255

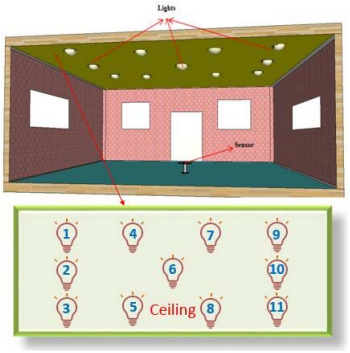

Fig. 2. First floor of the Arduino-based minihouse.

TABLE I
CORRESPONDING CURRENT VERSUS WITH THE CHANGING PWM VALUES IN LIGHTING SYSTEM

Control value	0	10	20	30	40	50	60	70	80
PWM(%)	0	3.922	7.843	11.76	15.69	19.61	23.53	27.45	31.37
Current(*mA*)	0	1.90	3.80	5.69	7.60	9.50	11.43	13.35	15.26
Control value	90	100	110	120	130	140	150	160	170
PWM(%)	35.29	39.22	43.14	47.06	50.98	54.90	58.82	62.75	66.67
Current(*mA*)	17.21	19.10	21.08	23.01	24.97	26.92	28.90	30.81	32.82
Control value	180	190	200	210	220	230	240	250	255
PWM(%)	70.59	74.51	78.43	82.35	86.27	90.20	94.12	98.04	100
Current(*mA*)	34.69	36.73	38.73	40.70	42.70	44.60	46.60	48.50	49.40

(i.e., $255 = 2^8 - 1$). After Arduino receives υ, the corresponding PWM value for each-group lighting equipment is derived through $0 \leq PWM = \upsilon/255 \leq 1$. To investigate clearly the minimal LC tracking, υ, PWM, and the current's measured values (i.e., I measured by the multimeter) are given in Table I. Obviously, the fit formula $\hat{I} = 0.1944\ \upsilon - 0.2054$ can be acquired from Table I. It should be noted that $\hat{I}$ denotes the fit value of the current. Since the PWM value (i.e., duty ratio) is $PWM = \upsilon/255$ and the output reference voltage of PWM is 5 V, the effective voltage value can be derived as Vol_Effect$= 5(PWM)^{1/2}$. By fitting the relationship between Vol_Effect and I, the Vol_Effect (unit: V) is linear with I (unit: mA) when $I > 10$ mA passes through the LED. Hence, the power can be approximated by $P = k \times (0.1944\ \upsilon - 0.2054)^2$, where k represents a constant. Since the actually electricity consumption (W) refers to the energy consumption in a certain period of time, electricity consumption can be derived by $W = \int_0^{\mathrm{t}} P(t)dt$. It is obvious that the power will be maintained at the point when finding the minimum power point, so that the electricity consumption in the same time can keep relatively low. To easily show the minimizing electricity consumption, we call the power as LC. Hence, the track of the minimal power point is considered to reduce the electricity consumption.

In this paper, the main purpose is to achieve the minimal LC tracking by controlling the luminance of multigroup lighting equipment (i.e., n group), respectively, while the indoor illumination track correctly the required level of illumination. As depicted in Fig. 1, the considered optimal method should contains two loops: 1) *the required level of illumination control loop* is to achieve the required level of illumination and 2) *minimal LC tracking loop* is to ensure the track of the minimal LC. In the control method, υ_w means the total PWM signal that guarantees the required level of illumination. In addition, υ_w is cut into n groups $\upsilon_i, i = 1, \ldots, n$, to adjust n group lighting equipment, respectively. The PWM signal υ_i is employed in i group lighting equipment. Based on Remark 1, the fit formula $\hat{I}_i = 0.1944\ \upsilon_i - 0.2054$ is applied for approximating the current value I_i, which is offered for the corresponding i group lighting equipment. Hence, LC E is summarized as

$$\begin{aligned} E &\approx \hat{I}_1^2 + \hat{I}_2^2 + \cdots + \hat{I}_n^2 \\ \hat{I}_i &= 0.1944\upsilon_i - 0.2054, \quad i = 1, \ldots, n \end{aligned} \tag{1}$$

in which $\upsilon_w = \sum_{i=1}^{n} \upsilon_i$ and $0 \leq \upsilon_i \leq \upsilon_w$. E in (1) is defined as an objective function in this paper. Although there is no definite physical meanings for this objective function, it should be easily analyzed how to realize the energy-saving via the proposed method. Furthermore, let us define $\upsilon_i = \omega_i \upsilon_w$, $(i = 1, \ldots, n-1)$, $\upsilon_n = (1 - \sum_{i=1}^{n-1} \omega_i)\upsilon_w$, where $\omega_i, i = 1, \ldots, n-1$ denote the proportional parameters satisfying $1 \geq 1 - \sum_{i=1}^{n-1} \omega_i \geq 0$ and $1 \geq \omega_i \geq 0$. Furthermore, E can be displayed by

$$\begin{aligned} E = &\sum_{i=1}^{n-1} (0.1944\omega_i \upsilon_w - 0.2054)^2 \\ &+ \left\{ 0.1944\left(1 - \sum_{i=1}^{n-1} \omega_i\right)\upsilon_w - 0.2054 \right\}^2. \end{aligned} \tag{2}$$

Apparently, the minimal LC tracking problem exists in (2), which could be solved by regulating ω_i, respectively. In the meanwhile, the required level of illumination can be ensured by controlling υ_w. Hence, the main goal is to pull E toward the minimal LC $E^\natural$, and then lock it into the small area of $E^\natural$.

To investigate the main problem, the 11 LEDs can be split into three group lighting equipment, without loss of generality, where the first group consists of the sixth LED; the second group contains the fourth LED, the fifth LED, the seventh LED, and the eighth LED; and the third-group involves the rest of LEDs, as shown in Fig. 2. There are $\omega_i, (i = 1, 2)$ satisfying $1 \geq 1 - \sum_{i=1}^{2} \omega_i \geq 0$ and $1 \geq \omega_i \geq 0$, which can be adjusted separately to cut down E. Next, the real-time optimal control method is designed to guarantee the actualization of the required level of illumination and the track of minimal LC.

To verify the application effect of the proposed control algorism, the first step is to illustrate that *the required level of illumination control loop* should guarantee the actualization of the required level of illumination. Next, the illuminance value of 60 lx is selected as the required level of illumination in the following example. As displayed in Fig. 3, the indoor illumination under PID does maintain 60 lx as predicted. In the meanwhile, E versus $\omega_i, (i = 1, 2)$ characteristics are depicted in Fig. 4, whereas the required level of illumination is guaranteed. Furthermore, the corresponding variety in the $\omega_1 - \omega_2$ plane is displayed in Fig. 5. As shown in Figs. 4 and 5, there is a minimal LC $E^\natural = 1.7318$ while $\omega_1^\natural, \omega_2^\natural$ are 0.5 and 0.3632. It should also be noticed that $E^\natural + 5\% \geq E$ while $\omega_i, (i = 1, 2)$ are in the light gray area of Fig. 5

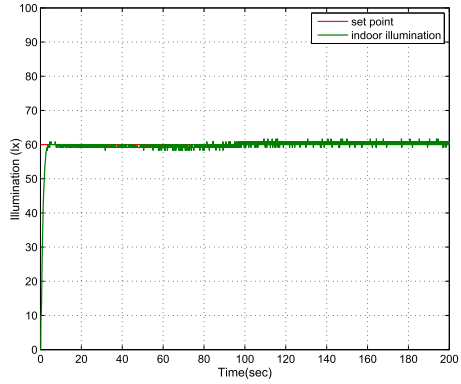

Fig. 3. Indoor illumination under PID in the Arduino-based minihouse.

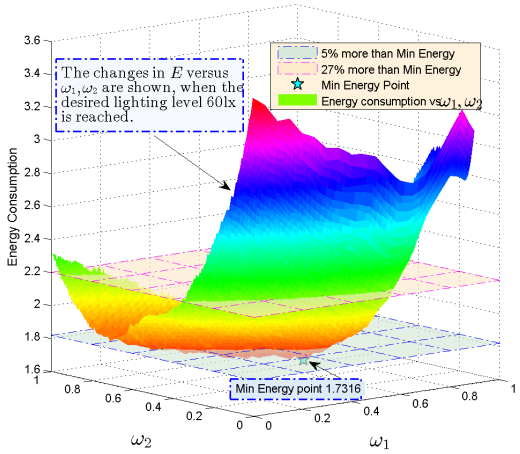

Fig. 4. Varying of E versus $\omega_i, (i = 1, 2)$, while maintaining the required level of illumination.

(i.e., $\omega_1 \in (0.099, 0.55)$, $\omega_2 \in (0.293, 0.63)$). Moreover, $E^\natural + 27\% \geq E$ while $\omega_i, (i = 1, 2)$ are stuck at this figure's purple area [i.e., $\omega_1 \in (0, 0.684)$, $\omega_2 \in (0.091, 0.96)$].

Actually, the objective of *minimal LC tracking loop* is to drive $\omega_i, (i = 1, 2)$ toward $\omega_i^\natural$ and stuck around it as well, to track the minimal LC efficiently. What is more, considering the general case (i.e., not just for three group lighting equipment), the proposed second loop is established to achieve the track of the minimal LC $E^\natural$ while $\omega_i, (i = 1, \ldots, n-1)$ can converge to $\omega_i^\natural$. Hence, *the minimizing LC control loop* is called as a multivariate ESC matter.

Remark 2: In earlier research studies, we designed SM-ESC for two group lighting equipment to realize the track of minimal LC [21], [22], so only one ω_1 is variable in this case. In other words, SM-ESC mentioned earlier can just be employed in the SISO lighting plant. However, considering the complicated hybrid lighting system with more than two group lighting equipment, some effective multivariate optimal algorithms are required to realize the track of minimal LC. In order to fulfill the purpose, a multivariate ESC will be designed to achieve the minimal LC as well as the required level of illumination.

III. MISO Extremum Seeking Scheme

Consider the following nonlinear system:

$$\dot{x} = \psi(x, \theta), \quad y = E(x) \tag{3}$$

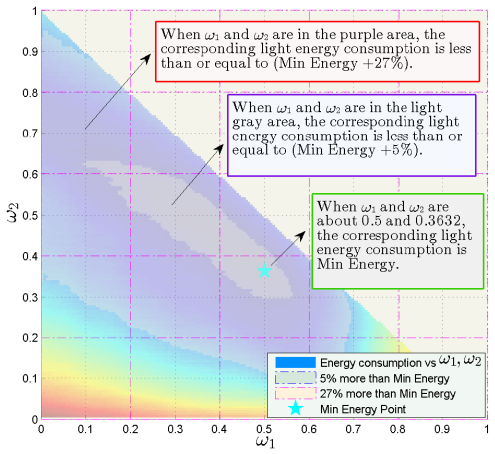

Fig. 5. Varying of E versus $\omega_i, (i = 1, 2)$ in the $\omega_1 - \omega_2$ plane.

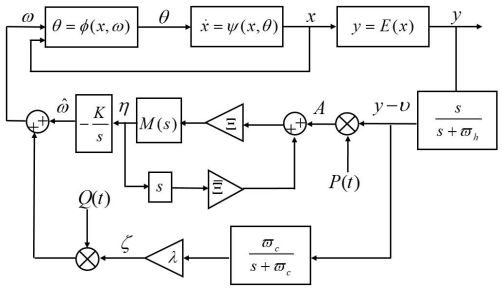

Fig. 6. Block diagram of MISO-ESCDDS.

where $x \in R^l$, $y \in R$, and $u \in R^n$. The function $\psi : R^l \times R^n \to R^l$ and $E : R^l \to R$ are smooth. In addition, system (3) is rewritten as $\dot{x} = \psi(x, \phi(x, \omega))$, when adopting the control input $\theta = \phi(x, \omega), \omega \in R^n$. The aim is to minimize y but without claiming the related information of either E or $\omega^\natural$. Next, the following assumptions considered in [23] and [26] are applied for the above-mentioned system.

Assumption 1: $\psi(x, \phi(x, \omega)) = 0$ can be guarantte, if $x = \iota(\omega)$ containing the smooth function $\iota : R^n \to R^l$.

Assumption 2: The equilibrium point $x = \iota(\omega)$ of the system (3) via $u = \phi(x, \omega)$ is locally exponentially stable.

For $y = E(\iota(\omega)) = \bar{E}(\omega)$, assume that there is a only minimal point $\bar{E}(\omega^\natural)$ at $\omega^\natural \in R^n$. This purpose is to minimize y without claiming the related info of either $E, \omega^\natural$ or ι. Hence, we apply the following assumption in the minimal point tracking problem.

Assumption 3: There is a only $\omega^\natural$ enabling $\partial \bar{E}(\omega^\natural)/\partial\omega = 0$ and $\partial^2 \bar{E}(\omega^\natural)/\partial\omega^2 = H > 0$, which $H^T = H$.

In the following, we will propose a MISO ESC with diminishing dither signal (MISO-ESCDDS) to search the minimal point $y^\natural = \bar{E}(\omega^\natural)$. To actualize this purpose, we present the frame of MISO-ESCDDS (as shown in Fig. 6), which contains

$$\begin{aligned} M(s) &= \operatorname{diag}\left\{\frac{\chi_1}{s+\chi_1}, \cdots, \frac{\chi_n}{s+\chi_n}\right\}, k = \operatorname{diag}\{k_1, \ldots, k_n\} \\ \Xi &= \operatorname{diag}\{\Xi_1, \ldots, \Xi_n\}, \bar{\Xi} = \operatorname{diag}\left\{\bar{\Xi}_1, \ldots, \bar{\Xi}_n\right\} \\ P(t) &= \left[\frac{2\sin\varpi_1 t}{\epsilon_1} \; \frac{2\sin\varpi_2 t}{\epsilon_2} \; \cdots \; \frac{2\sin\varpi_n t}{\epsilon_n}\right]^T \\ Q(t) &= \left[\epsilon_1 \sin\varpi_1 t \; \epsilon_2 \sin\varpi_2 t \; \cdots \epsilon_n \sin\varpi_n t\right]^T \end{aligned} \tag{4}$$

in which $\lambda, \chi_i, k_i, \epsilon_i, \Xi_i, \bar{\Xi}_i > 0$ and the frequencies $\varpi_i > 0, (i = 1, 2, \ldots, n)$. χ_i, Ξ_i, and $\bar{\Xi}_i$ are selected to guarantee $1 - \chi_i \Xi_i \bar{\Xi}_i > 0$. Moreover, we request $\varpi_l \neq \varpi_m$ and $\varpi_l + \varpi_m \neq \varpi_n$ for different l, m, n. From Fig. 6, the system (3) with MISO-ESCDDS is represented as

$$\begin{aligned}
\frac{dx}{dt} &= \psi(x, \phi(x, \hat{\omega} + \zeta Q(t)) \\
\frac{d\hat{\omega}}{dt} &= -k\eta \\
\frac{d\eta}{dt} &= (I - \Xi \bar{M} \bar{\Xi})^{-1}(\Xi \bar{M}(y - \nu) P(t) - \bar{M}\eta) \\
\frac{d\zeta}{dt} &= \lambda \varpi_c (y - \nu) - \omega_c \zeta \\
\frac{d\nu}{dt} &= \varpi_h (y - \nu)
\end{aligned} \tag{5}$$

where $\varpi_c, \varpi_h > 0$, and $\bar{M} = \text{diag}\{\chi_1, \chi_2, \ldots, \chi_n\}$. The parameter λ is selected to guarantee $\zeta > 0$. To analyze the stability of the scheme, $k, \varpi_h, \varpi_c, \varpi_i, \chi_i, (i = 1, 2, \ldots, n)$ are chosen as $\varpi_i = \mu \breve{\varpi}_i = O(\mu)$, $\varpi_h = \mu \varpi_H = \mu \vartheta \breve{\varpi}_H = O(\mu\vartheta)$, $\varpi_c = \mu \varpi_C = \mu\varepsilon\vartheta \breve{\varpi}_C = O(\mu\varepsilon\vartheta)$, $k = \mu K = \mu\varepsilon\vartheta \breve{K} = O(\mu\varepsilon\vartheta)$, $\bar{M} = \mu \hat{M} = \mu\varepsilon\vartheta \breve{M} = O(\mu\varepsilon\vartheta)$, in which ε, ϑ, and μ mean small positive constants. $\breve{\varpi}_C$ and $\breve{\varpi}_H$ denote $O(1)$ positive constants. $\breve{K} \in R^{n\times n}$ and $\breve{M} \in R^{n\times n}$ represent diagonal matrices that possess $O(1)$ positive constants. $\breve{\varpi}_i$ is a rational number. One possible selection is shown in [23] as $\breve{\varpi}_i \notin \{\breve{\varpi}_j, \frac{1}{2}(\breve{\varpi}_j + \breve{\varpi}_k), \breve{\varpi}_j + 2\breve{\varpi}_k, \breve{\varpi}_j + \breve{\varpi}_k \pm \breve{\varpi}_l\}$. Define $\bar{\omega} = \hat{\omega} - \omega^\natural$ and $\tilde{\nu} = \nu - \bar{E}(\omega^\natural)$, in the time scale $\gamma = \mu t$, this system (5) can be further written as

$$\begin{aligned}
\varpi \frac{dx}{d\gamma} &= \psi(x, \phi(x, \omega^\natural + \bar{\omega} + \zeta \tilde{Q}(\gamma)) \\
\frac{d}{d\gamma}\begin{bmatrix} \bar{\omega} \\ \eta \\ \zeta \\ \tilde{\nu} \end{bmatrix} &= \vartheta \begin{bmatrix} -\varepsilon \breve{K}\eta \\ \varepsilon W^{-1}[\Xi \breve{M}(h(x) - \bar{E}(\omega^\natural) - \tilde{\nu})\tilde{P}(\gamma) - \breve{M}\eta] \\ \varepsilon[\lambda \breve{\varpi}_C (h(x) - \bar{E}(\omega^\natural) - \tilde{\nu}) - \breve{\varpi}_C \zeta] \\ \breve{\varpi}_H (h(x) - \bar{E}(\omega^\natural)) - \breve{\varpi}_H \tilde{\nu} \end{bmatrix}
\end{aligned} \tag{6}$$

in which $\tilde{Q}(\gamma) = Q(t/\mu)$, $\tilde{P}(\gamma) = P(/t/\mu)$, and $W = I - \mu\varepsilon\vartheta \Xi \breve{M} \bar{\Xi}$. Then, we focus on the stability of this system (6).

Theorem 1: For the system (5) via MISO-ESCDDS in the presence of Assumptions 1–3. $\exists\ \mu^\natural, \varepsilon^\natural, \vartheta^\natural, \alpha_i^\natural > 0, (i = 1, \ldots, n)$ such that $\forall \mu \in (0, \mu^\natural), \forall \varepsilon \in (0, \varepsilon^\natural), \forall \vartheta \in (0, \vartheta^\natural)$, and $\forall \alpha_i \in (0, \alpha_i^\natural), \exists$ a neighborhood of $(x, \hat{\omega}, \eta, \zeta, \nu) = (\iota(\omega^\natural), \omega^\natural, 0, 0, \bar{E}(\omega^\natural))$ such that $(x(t), \hat{\omega}(t), \eta(t), \zeta(t), \nu(t))$ exponentially converges to $(\iota(\omega^\natural), \omega^\natural, 0, 0, \bar{E}(\omega^\natural))$. In addition, $y(t)$ can exponentially converge to $\bar{E}(\omega^\natural)$.

Proof: See Appendix B.

Remark 3: For the controlled system (5), the equilibrium of the corresponding average system is obtained in the proof of Theorem 1. $\epsilon_i \zeta, i = 1, \ldots, n$ are the amplitudes of the dither signal $Q(t)$. From the framework of MISO-ESCDDS in Fig. 6, we have that ζ could be a large value during the initial time interval when $\bar{\omega}$ has a large initial value. Compared with the constant amplitudes in the MISO gradient- and Newton-based ESC (see [23], [24], and [26]), the amplitudes of MISO-ESCDDS can be manipulated to enlarge the seeking region to avoid effectively arriving at the local extrema. Furthermore, since that ζ is proven to exponentially converge to the origin, we can conclude that $\bar{\omega}$ exponentially converge to zero. That is, y must be close to $\bar{E}(\omega^\natural)$. Hence, the proposed MISO-ESCDDS can improve the seeking speed, domain of accuracy, and attraction of the extremum seeking scheme. The following experiments are applied to identify the benefits of the proposed MISO-ESCDDS.

Remark 4: There exist few ESCs' applications for lighting systems with multilighting equipment. The Newton method in [27] has been implemented in MISO lighting systems. The FO gradient-based ESC in (see [6], [28]) has been to realize the track of minimal LC. Both of Newton- and gradient-based ESCs can be thought as the feasible methods for minimal LC tracking problems, nevertheless, they have a possibility to bring about the unwelcome oscillations due to the changeless amplitudes of the dither signal. Actually, these amplitudes are the primary parameters that determine both oscillations and track efficiency. Newton- and gradient-based ESCs with the large amplitudes can reach the minimal LC quickly, but with large oscillations. However, the small amplitudes can decrease oscillations but slow down the LC's convergence speed. This calls for the tradeoff between oscillations and track efficiency. Hence, it is important to improve the control performance of multivariate ESC, this is the motivation of our paper. Since ζ is proven to exponentially converge to the origin, the proposed ESC is developed to ensure the amplitude of the dither signal converge exponentially to zero by making the amplitudes change with the extremum estimation error. The proposed frame helps to improve search speed for the minimal LC and remove the steady-state oscillations.

Remark 5: The frame of MISO-ESCDDS includes $\Xi, \bar{\Xi}, M(s)$ and a differentiator. From Fig. 6, we have $d\hat{\omega}/dt = -k\eta$ with $\eta = M(s)\Xi(A + \bar{\Xi}\dot{\eta})$. Setting $\eta = (\eta_1, \eta_2, \ldots, \eta_n)^T$ and $A = (A_1, A_2, \ldots, A_n)^T$, we obtain $\eta_i = [(\Xi_i\chi_i)/(s + \chi_i)](\bar{\Xi}_i \dot{\eta}_i + A_i) \Rightarrow \dot{\eta}_i = (\Xi_i \chi_i A_i - \chi_i \eta_i)/(1 - \Xi_i \chi_i \bar{\Xi}_i)$. Thus, we have $d\hat{\omega}/dt = -k\eta$ and $d\eta/dt = (I - \Xi M \bar{\Xi})^{-1} \Xi M A - (I - \Xi M \bar{\Xi})^{-1} M\eta$ for MISO-ESCDDS. Clearly, k and η should affect the tracking speed of MISO-ESCDDS. Based on the constant matrix $(I - \Xi M \bar{\Xi})^{-1} M$, one can conclude that $\dot{\eta}$ involves a proportional-rate item $-(I - \Xi M \bar{\Xi})^{-1} M\eta$, which can draw quickly η to stable point while $\eta(t)$ is great. It is useful to raise the convergence speed and without boosting the oscillations performance.

IV. Experimental Results

As depicted in Fig. 7, the developed MISO-ESCDDS will be implemented in lighting experiment of minihouse described in Section II, to guarantee the track of the minimal LC.

Case 1: The 11 LEDs are separated into three group lighting equipment, which has been illustrated in Section II in detail. For the case, MISO-ESCDDS is applied for minimizing the LC E written as

$$\begin{aligned}
E = \sum_{i=1}^{2} (0.1944 \omega_i v_w - 0.2054)^2 \\
+ \left\{ 0.1944 \left(1 - \sum_{i=1}^{2} \omega_i \right) v_w - 0.2054 \right\}^2
\end{aligned} \tag{7}$$

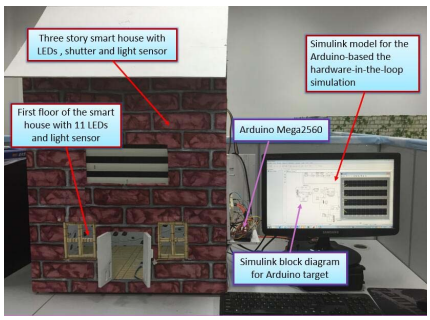

Fig. 7. Arduino-based minihouse.

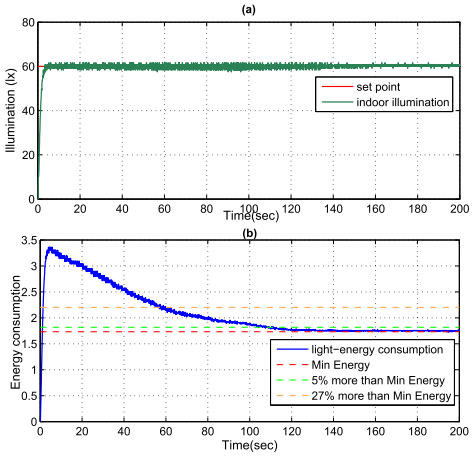

Fig. 8. (a) Illumination via PID in the minihouse. (b) E under MISO-ESCDDS.

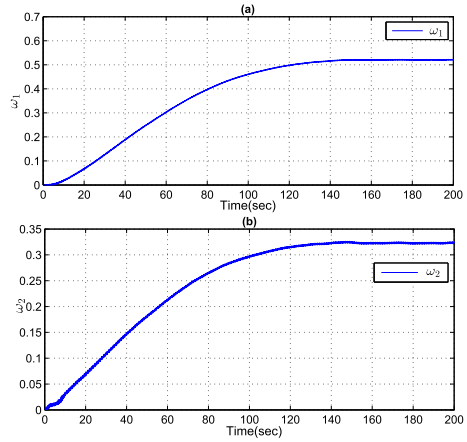

Fig. 9. Time responses of ω_i, $(i = 1, 2)$ under the proposed MISO-ESCDDS. The time response of (a) ω_1 and (b) ω_2.

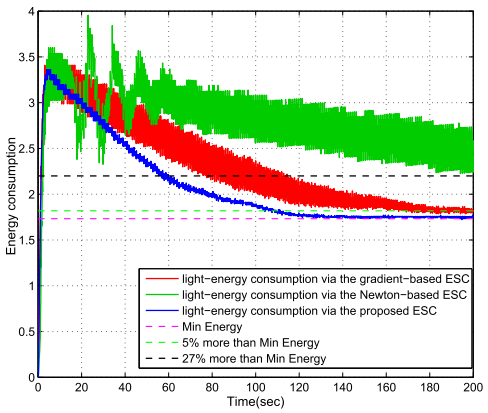

Fig. 10. Comparison among E via MISO-ESCDDS, the Newton- and gradient-based ESCs, while keeping $60lx$.

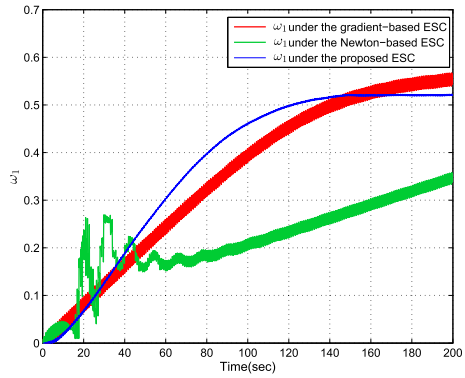

Fig. 11. Comparison among ω_1 under MISO-ESCDDS, the Newton- and gradient-based ESCs.

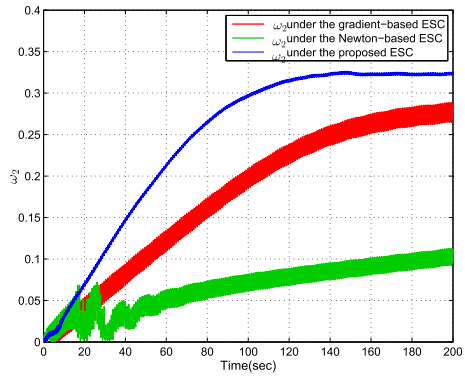

Fig. 12. Comparison among ω_2 under MISO-ESCDDS, the Newton- and gradient-based ESCs.

where $2 \leq 1 - \sum_{i=1}^{2} \omega_i \leq 1$ and $1 \geq \omega_i \geq 0$. It is noted that ω_i, $(i = 1, 2)$ via MISO-ESCDDS will be manipulated to realize the minimal LC tracking, meanwhile υ_w via PID will be controlled to ensure the actualization of the required level of illumination.

Next, the experiment will employ MISO-ESCDDS with $k = 10^{-4}\text{diag}\{2, 1\}$, $\bar{M} = \text{diag}\{0.1, 0.2\}$, $\Xi = \text{diag}\{1, 1.5\}$, $\bar{\Xi} = \text{diag}\{0.1, 0.1\}$, $\hat{\omega}(0) = [0, 0]^T$, $\varpi_1 = \varpi_2 = 30$, $\epsilon_1 = \epsilon_2 = 0.01$, $\varpi_h = 0.0001$, $\lambda = 0.01$, $\varpi_c = 0.2$. As illustrated in Fig. 8(a), the indoor illumination reaches the required level of illumination $60lx$, in the presence of PID, with the parameters $c_p = 0.3$, $c_i = 2$ and $c_d = 0.1$. Meanwhile, LC E via MISO-ESCDDS can track $E^\natural = 1.7318$ and then be often less than $E^\natural + 5\%$, as shown in Fig. 8(b). Fig. 9 displays that ω_i, $(i = 1, 2)$ under MISO-ESCDDS approaches to $\omega_1^\natural$, $\omega_2^\natural$ and stuck in the domain of $E^\natural + 5\%$, as depicted in Fig. 5. Hence, the proposed method including MISO-ESCDDS can guarantee the actualization of the required level of illumination and the track of minimal LC, as shown in Figs. 8 and 9.

To verify the potential benefits of MISO-ESCDDS, the lighting experiment is repeated for the Newton- and

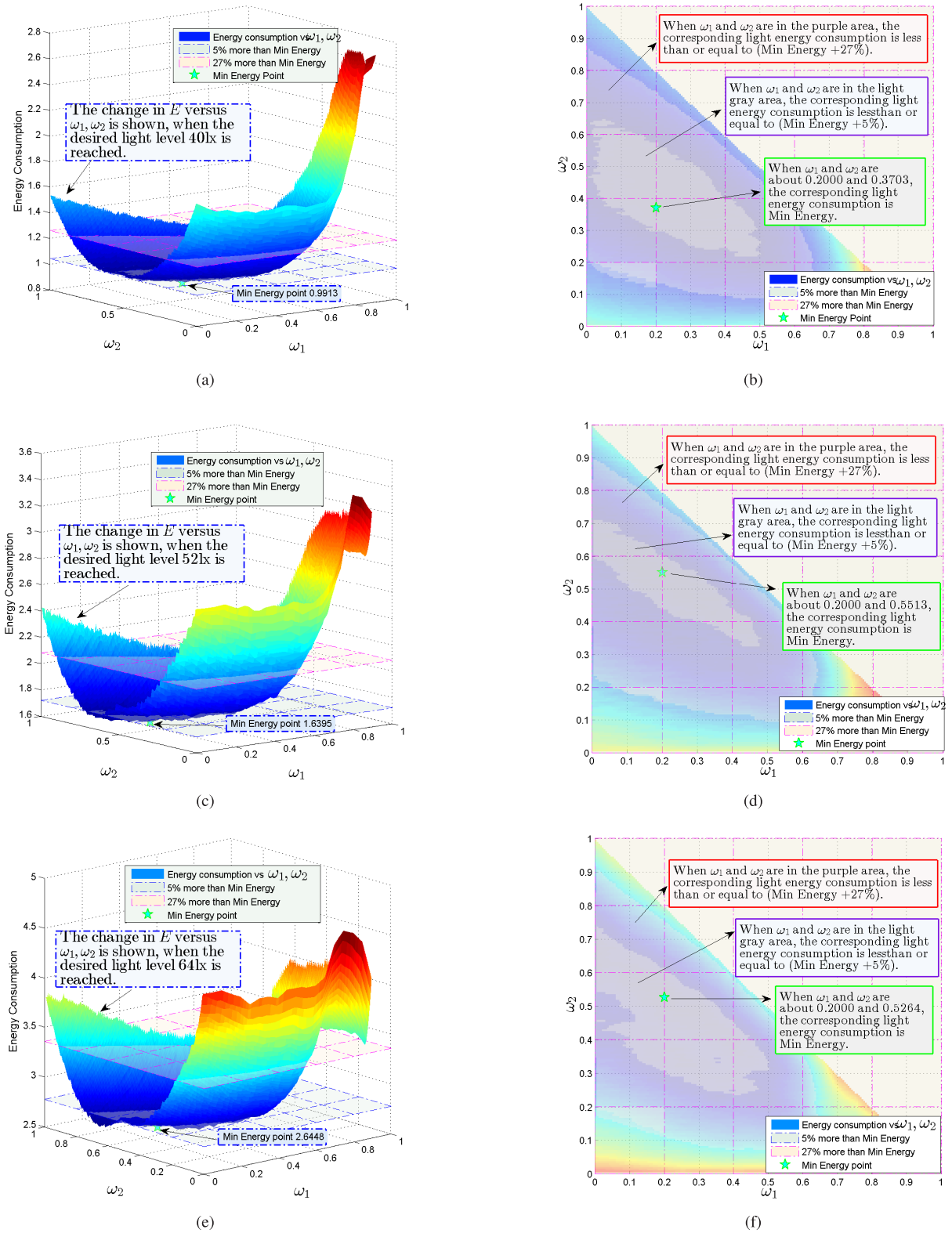

Fig. 13. Varying of E versus $\omega_i, (i = 1, 2)$, when keeping $40lx, 52lx, 64lx$, respectively. (a) Varying of E versus $\omega_i, (i = 1, 2)$, when keeping $40lx$. (b) Varying of E versus $\omega_i, (i = 1, 2)$, when keeping $52lx$. (c) Varying of E versus $\omega_i, (i = 1, 2)$ in the $\omega_1 - \omega_2$ plane. (d) Varying of E versus $\omega_i, (i = 1, 2)$ in the $\omega_1 - \omega_2$ plane. (e) Varying of E versus $\omega_i, (i = 1, 2)$,when keeping $64lx$. (f) Varying of E versus $\omega_i, (i = 1, 2)$ in the $\omega_1 - \omega_2$ plane.

Gradient-based ESCs in [23]. All common parameters of the above-mentioned three ESCs are same, excluding the gain k_N of the Newton-based ESC. From [23] and [26], the gain k is chosen by $k = k_G = k_N\Gamma(0)$, where k_G and k_N separately represent here the gains of the corresponding Newton- and gradient-based ESCs. For the Newton-based ESC, the other parameters are $k_N = \text{diag}\{4, 0.8\}$, $\Gamma^{-1}(0) = 10^4\text{diag}\{2, 0.8\}$, $\varpi_r = 0.01$. Fig. 10 shows the comparison of LCs via MISO-ESCDDS, the Newton- and gradient-based ESCs. Moreover, Figs. 11 and 12 depict the corresponding

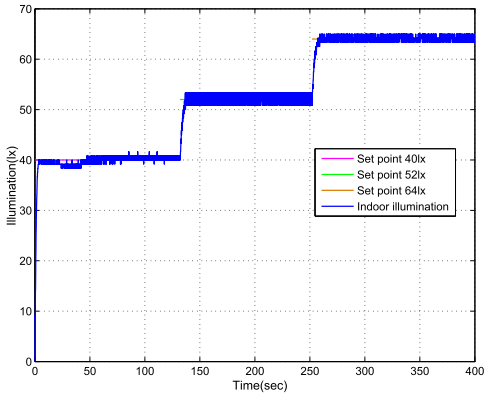

Fig. 14. Illumination under PID of the minihouse.

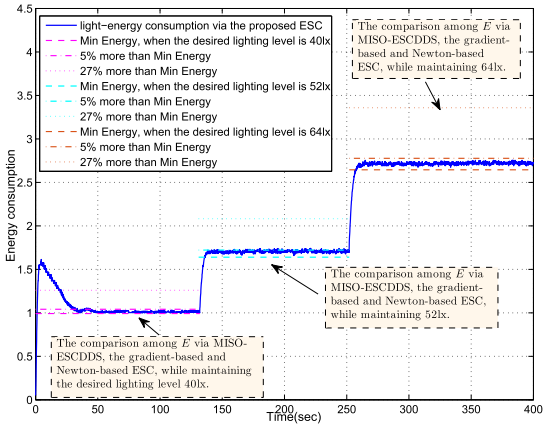

Fig. 15. E under MISO-ESCDDS, while maintaining the changing required level of illumination.

ω_1, ω_2 via MISO-ESCDDS, the Newton- and gradient-based ESCs. These figures show that E via MISO-ESCDDS can have higher accuracy and faster speed than that of the multivariate Newton- and gradient-based ESCs. These results verify the potential benefits of the developed MISO-ESCDDS.

Case 2: The 11 LEDs are also separated into three group lighting equipment, which are same as Case 1. The varying required level of illumination is selected from $40lx$ to $52lx$ to $64lx$. The indoor illumination can track the changing required level of illumination, in the presence of PID with $c_p = 0.2, c_i = 2, c_d = 0.1$. At the same time, E versus $\omega_i, (i = 1, 2)$ are shown in Fig. 13(a)–(c), respectively. This figure displays that there is $E^\natural = 0.9913$ when $\omega_i^\natural, (i = 1, 2)$ are 0.2000 and 0.3703 in Fig. 13(a). There is $E^\natural = 1.6395$ when $\omega_i^\natural, (i = 1, 2)$ are 0.2000 and 0.5513 in Fig. 13(b), there is $E^\natural = 2.6448$ when $\omega_i^\natural, (i = 1, 2)$ are 0.2000 and 0.5264 in Fig. 13(c). Next, MISO-ESCDDS is employed to guarantee that E can converge to $E^\natural$ through regulating $\omega_i, (i = 1, 2)$, while maintaining the varying required level of illumination from $40lx$ to $64lx$.

Then, the developed MISO-ESCDDS is adopted with $k = 10^{-4}\text{diag}\{6, 4\}$, $\bar{M} = \text{diag}\{0.2, 0.2\}$, $\Xi = \text{diag}\{2, 3\}$, $\bar{\Xi} = \text{diag}\{0.1, 0.1\}$, $\hat{\omega}(0) = [0, 0]^T$, $\epsilon_1 = \epsilon_2 = 0.01$, $\varpi_1 = \varpi_2 = 30$, $\varpi_h = 0.0002$, $\lambda = 0.01$, $\varpi_c = 0.1$. Fig. 14 displays that the indoor illumination tracks the varying required level of illumination from $40lx$ to $64lx$, in the presence of PID. Fig. 15 shows the corresponding LC E under MISO-ESCDDS. This figure shows that E can track $E^\natural = 0.9913$ and then mostly stay in the domain of $E^\natural + 5\%$, whereas the required level of illumination is $40lx$. Then, E continues to track $E^\natural = 1.6395$ and then mostly stuck in the domain of $E^\natural + 5\%$, while the required level of illumination is raised to $52lx$. Finally, E can track $E^\natural = 2.6448$ and then mostly stay in the domain of $E^\natural + 5\%$, when the required level of illumination is $64lx$.

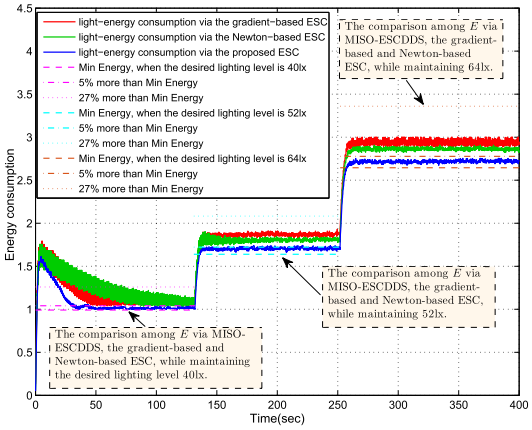

Fig. 16. Comparison among E under MISO-ESCDDS, the Newton- and gradient-based ESCs, while maintaining the changing required level of illumination.

To further verify the potential benefits of MISO-ESCDDS, the lighting experiment is also repeated for the Newton- and gradient-based ESCs in [23]. All common parameters of the above-mentioned three ESCs are same, except for k_N. From [23] and [26], the gain k is chosen by $k = k_G = k_N\Gamma(0)$. From $k = k_G = k_N\Gamma(0)$ in (see [23] and [26]), $k_N = \text{diag}\{6, 4\}$ and $\Gamma^{-1}(0) = 10^4\text{diag}\{1, 1\}$ are chosen. Fig. 16 displays the comparison among MISO-ESCDDS, the Newton- and gradient-based ESCs. This figure shows that E in the presence of MISO-ESCDDS can have a faster track of the minimal LC while guaranteeing the control accuracy. These results verify the potential benefits of MISO-ESCDDS, even when maintaining the varying required level of illumination.

Remark 6: Hence, for saving more electrical energy cost on the premise that the required level of illumination of the target location is achieved. This paper develops a real-time optimal control method to realize the track of the minimal LC by independently control the multilighting equipment. Considering the variability of ambient illumination environment, an adaptive real-time lighting control method is designed to track the minimal LC point and achieve the required level of illumination simultaneously. To have a better understanding of the proposed MISO-ESCDDS and its stability property, the structure and function of the MISO hybrid lighting control systems are carefully described and discussed in this paper. Moreover, on condition that the target location with designated lighting equipment is determined, the issue of minimal energy consumption point tracking is also studied in detail. In the future, the division of object regions and the distribution of the corresponding sensors will become the emphasis of our works.

Remark 7: Since that the minihouse adopts the pure copper wires with 0.85 mm^2 cross section area, the calculated

direct-current line resistance at 20 °C is about 0.0208 Ω/m based on basis physical parameters in (see [29]–[32]), which is similar as manufacturer's instructions. Because the wire lengths of each branch are no longer than 0.5 m, the line electric resistance is usually less than 0.0104 Ω. Compared with LED resistance 74 Ω, the line resistance is very small and can be ignored in (1). Moreover, we can substitute the measured line resistance value into the proposed model-less algorithm, even if the line resistance cannot be ignored in some applications. Hence, the proposed algorithm is still available in complex application.

V. Conclusion

This paper proposed the real-time optimal control technique to improve energy-saving efficiency, for the lighting system with multilighting equipment. The control method contained MISO-ESCDDS which realizes the actualization of the minimal LC tracking by adjusting, respectively, the multilighting equipment, and PID which is applied to actualize the required level of illumination. The proposed MISO-ESCDDS can be useful for increasing the search speed for the minimal LC, and avoiding the steady-state oscillations for the lighting system. Experimental results including comparisons with the Newton- and gradient-based ESC verified the effectiveness and advantages of the developed MISO-ESCDDS.

Appendix A

Lemma 1 [33]: Consider $\dot{\varrho}_1 = \Lambda_1\varrho_1 + \bar{l}_1(\varrho_1,\varrho_2), \dot{\varrho}_2 = \Lambda_2\varrho_2 + \bar{l}_1(\varrho_1,\varrho_2)$, where the twice continuously differentiable nonlinear functions $\bar{l}_1(\varrho_1,\varrho_2)$, $\bar{l}_2(\varrho_1,\varrho_2)$ are satisfied $\bar{l}_i(0,0) = 0, [\partial\bar{l}_i/\partial\varrho_1](0,0) = 0, [\partial\bar{l}_i/\partial\varrho_2](0,0) = 0$ for $i = 1, 2$. If all eigenvalues of Λ_1 and Λ_2 possess separately zero real parts and negative real parts, $\exists$ a continuously differentiable function $p(\varrho_1)$ and $\rho > 0$, such that $\varrho_2 = p(\varrho_1)$ become a center manifold, defined for all $\rho > \|\varrho_1\|$.

Lemma 2 [33]: If there exists a function $\bar{\phi}(\varrho_1)$ that is continuously differentiable and satisfies $\bar{\phi}(0) = 0$ and $[\partial\bar{\phi}/\partial\varrho_1](0) = 0$, such that $N(\bar{\phi}(\varrho_1)) = O(\|\varrho_1\|^{\iota})$ for some $\iota > 1$, then one can obtain that $p(\varrho_1) = \bar{\phi}(\varrho_1) + O(\|\varrho_1\|^{\iota})$ for small enough $\|\varrho_1\|$, and the reduced system is expressed by $\dot{\varrho}_1 = \Lambda_1\varrho_1 + \bar{l}_1(\varrho_1, \bar{\phi}(\varrho_1)) + O(\|\varrho_1\|^{\iota+1})$.

Lemma 3 [33]: In the presence of the conditions in Lemma 1, the systems $\dot{\varrho}_1 = \Lambda_1\varrho_1 + \bar{l}_1(\varrho_1,\varrho_2), \dot{\varrho}_2 = \Lambda_2\varrho_2 + \bar{l}_1(\varrho_1,\varrho_2)$ are exponentially stable, if the reduced system in Lemma 2 is exponentially stable.

Appendix B
Proof of Theorem 1

The proof of Theorem 1 will be given as follows.

First of all, x in (6) is fixed at $x = \iota(\omega^\natural + \bar{\omega} + \zeta\tilde{Q}(\gamma))$. Then, the reduced system can be gained

$$\frac{d}{d\gamma}\begin{bmatrix}\bar{\omega}_r\\ \eta_r\\ \zeta_r\\ \tilde{\nu}_r\end{bmatrix} = \vartheta\begin{bmatrix}-\varepsilon\check{K}\eta_r,\\ \varepsilon W^{-1}[\Xi\check{M}(\upsilon(\bar{\omega}_r+\zeta_r\tilde{Q}(\gamma))-\tilde{\nu}_r)\tilde{P}(\gamma)-\check{M}\eta_r]\\ \varepsilon[\lambda\check{\varpi}_C(\upsilon(\bar{\omega}_r+\zeta_r\tilde{Q}(\gamma))-\tilde{\nu}_r)-\check{\varpi}_C\zeta_r]\\ \check{\varpi}_H(\upsilon(\bar{\omega}_r+\zeta_r\tilde{Q}(\gamma)))-\check{\varpi}_H\tilde{\nu}_r\end{bmatrix} \tag{8}$$

in which $\upsilon(z)=\bar{E}(\omega^\natural + z) - \bar{E}(\omega^\natural)$ with $z = \bar{\omega}_r + \zeta_r\tilde{Q}(\gamma)$. One can acquire from Assumption 3

$$\upsilon(0)=0, \quad \frac{\partial\upsilon(0)}{\partial z} = 0, \ \frac{\partial^2\upsilon(0)}{\partial z^2} = H > 0. \tag{9}$$

Next, to apply averaging method, we select $\Omega = 2\pi \times LCM\{1/\check{\varpi}_i\}, i \in \{1,\cdots,n\}$ with the least common multiple LCM as the mutual period of ϖ_i, similar to the definition of the period in [23]. The average model of the reduced system can be acquired

$$\frac{d}{d\gamma}\begin{bmatrix}\bar{\omega}_r^a\\ \eta_r^a\\ \zeta_r^a\\ \tilde{\nu}_r^a\end{bmatrix} = \vartheta\begin{bmatrix}-\varepsilon\mu\check{K}\eta_r^a\\ \varepsilon\mu W^{-1}\left[\dfrac{\Xi\check{M}}{\Omega}\displaystyle\int_0^\Omega\upsilon(\bar{\omega}_r^a+\zeta_r^aQ(\varsigma))P(\varsigma)d\varsigma-\check{M}\eta_r^a\right]\\ \dfrac{\lambda\varepsilon\mu\check{\varpi}_C\int_0^\Omega\upsilon(\bar{\omega}_r^a+\zeta_r^aQ(\varsigma))d\varsigma}{\Omega}-\lambda\varepsilon\mu\check{\varpi}_C\tilde{\nu}_r^a-\varepsilon\mu\check{\varpi}_C\zeta_r^a\\ -\mu\check{\varpi}_H\tilde{\nu}_r^a+\dfrac{\mu\check{\varpi}_H}{\Omega}\displaystyle\int_0^\Omega\upsilon(\bar{\omega}_r^a+\zeta_r^aQ(\varsigma))d\varsigma\end{bmatrix}. \tag{10}$$

In addition, let the average equilibrium point $(\bar{\omega}_r^{a,e}, \eta_r^{a,e}, \zeta_r^{a,e}, \tilde{\nu}_r^{a,e})$ satisfy the following condition:

$$\eta_r^{a,e} = 0_{n\times1} \tag{11}$$

$$\frac{1}{\Omega}\int_0^\Omega\upsilon(\bar{\omega}_r^{a,e}+\zeta_r^{a,e}Q(\varsigma))P(\varsigma)d\varsigma = 0_{n\times1} \tag{12}$$

$$\frac{\lambda}{\Omega}\int_0^\Omega\upsilon(\bar{\omega}_r^{a,e}+\zeta_r^{a,e}Q(\varsigma))d\varsigma = \zeta_r^{a,e}+\lambda\tilde{\nu}_r^{a,e} \tag{13}$$

$$\frac{1}{\Omega}\int_0^\Omega\upsilon(\tilde{\omega}_r^{a,e}+\zeta_r^{a,e}Q(\varsigma))d\varsigma = \tilde{\nu}_r^{a,e}. \tag{14}$$

Based on the singular perturbation theory and center manifold methods in [33], the equivalent form of the system (10) can be derived

$$\begin{aligned}
\frac{d\bar{\omega}_r^a}{d\gamma} &= -\vartheta\varepsilon\mu\check{K}\eta_r^a\\
\frac{d\eta_r^a}{d\gamma} &= \vartheta\varepsilon\mu W^{-1}\left[\frac{\Xi\check{M}}{\Omega}\int_0^\Omega\upsilon(\bar{\omega}_r^a+\zeta_r^aQ(\varsigma))P(\varsigma)d\varsigma-\check{M}\eta_r^a\right]\\
\frac{d\zeta_r^a}{d\gamma} &= \vartheta\frac{\lambda\varepsilon\mu\check{\varpi}_C\int_0^\Omega\upsilon(\bar{\omega}_r^a+\zeta_r^aQ(\varsigma))d\varsigma}{\Omega}-\vartheta\varepsilon\mu\check{\varpi}_C(\lambda\tilde{\nu}_r^a-\zeta_r^a)\\
\frac{d\tilde{\nu}_r^a}{d\gamma} &= \vartheta\frac{\mu\check{\varpi}_H}{\Omega}\int_0^\Omega\upsilon(\bar{\omega}_r^a+\zeta_r^aQ(\varsigma))d\varsigma-\vartheta\mu\check{\varpi}_H\tilde{\nu}_r^a\\
\frac{d\varepsilon}{d\gamma} &= 0.
\end{aligned} \tag{15}$$

In addition, the system (12) can be expressed as

$$\dot{\varrho}_1 = \frac{d}{d\gamma}\begin{bmatrix}\bar{\omega}_r^a\\ \eta_r^a\\ \zeta_r^a\\ \varepsilon\end{bmatrix} = \Lambda_1\varrho_1 + \bar{l}_1(\varrho_1,\varrho_2) \tag{16}$$

$$\dot{\varrho}_2 = \frac{d\tilde{m}_r^a}{d\gamma} = \Lambda_2\varrho_2 + \bar{l}_2(\varrho_1,\varrho_2) \tag{17}$$

where

$$\varrho_1 = \begin{bmatrix} \bar{\omega}_r^a \\ \eta_r^a \\ \zeta_r^a \\ \varepsilon \end{bmatrix}, \quad \varrho_2 = \tilde{\nu}_r^a, \ \Lambda_1 = 0_{(2n+2)\times(2n+2)}$$

$$\bar{l}_1(\varrho_1, \varrho_2) = \vartheta \begin{bmatrix} -\vartheta\varepsilon\check{K}\eta_r^a \\ \vartheta\varepsilon\mu W^{-1}\left[\dfrac{\Xi\check{M}\int_0^\Omega \upsilon(\bar{\omega}_r^a+\zeta_r^a Q(\varsigma))P(\varsigma)d\varsigma}{\Omega} - \check{M}\eta_r^a\right] \\ \vartheta\varepsilon\mu\left[\dfrac{\lambda\check{\varpi}_C\int_0^\Omega \upsilon(\bar{\omega}_r^a+\zeta_r^a Q(\varsigma))d\varsigma}{\Omega} - \lambda\check{\varpi}_C\tilde{\nu}_r^a - \check{\varpi}_C\zeta_r^a\right] \\ 0 \end{bmatrix}$$

$$\Lambda_2 = -\vartheta\mu\check{\varpi}_H, \bar{l}_2(\varrho_1, \varrho_2) = \vartheta\frac{\mu\check{\varpi}_H}{\Omega}\int_0^\Omega \upsilon(\bar{\omega}_r^a+\zeta_r^a Q(\varsigma))d\varsigma.$$

One has that $\bar{l}_1(\varrho_1, \varrho_2), \bar{l}_2(\varrho_1, \varrho_2)$ are twice continuously differentiable and $\bar{l}_i(0,0) = 0, [\partial\bar{l}_i/\partial\varrho_1](0,0) = 0, [\partial\bar{l}_i/\partial\varrho_2](0,0) = 0, i = 1, 2$. Hence, from Lemma 1, $\exists$ is a continuously differentiable function $\bar{p}(\varrho_1)$ and $\bar{\rho} > 0$, such that $\varrho_2 = \bar{p}(\varrho_1)$ is a center manifold for (16), (17), defined for all $\bar{\rho} > \|\varrho_1\|$. Moreover, the function meets $\bar{p}(0) = 0, [d\bar{p}/d\varrho_1](0) = 0$. To investigate the stability of (15), we should obtain the approximation of $\varrho_2 = \bar{\phi}(\varrho_1)$. Let $N(\bar{\phi}(\varrho_1)) = (\partial\bar{\phi}/\partial\bar{\omega}_{r1}^a)(d\bar{\omega}_{r1}^a/dt) + \cdots + (\partial\bar{\phi}/\partial\bar{\omega}_{rn}^a)(d\bar{\omega}_{rn}^a/dt) + (\partial\bar{\phi}/\partial\eta_{r1}^a)(d\eta_{r1}^a/dt) + \cdots + (\partial\bar{\phi}/\partial\eta_{rn}^a)(d\eta_{rn}^a/dt) + (\partial\bar{\phi}/\partial\zeta_r^a)(d\zeta_r^a/dt) + \vartheta\mu\check{\varpi}_H\bar{\phi}(\varrho_1) - [(\vartheta\mu\check{\varpi}_H)/\Omega]\int_0^\Omega \upsilon(\bar{\omega}_r^a+\zeta_r^a Q(\varsigma))d\varsigma$. From Taylor's expansion of $\upsilon(\bar{\omega}_r^a + \zeta_r^a Q(\varsigma))$, one has $(1/\Omega)\int_0^\Omega \upsilon(\bar{\omega}_r^a + \zeta_r^a Q(\varsigma))d\varsigma = (1/2)\sum_{J=1}^n\sum_{i=1}^n H_{iJ}\bar{\omega}_{ri}^a\bar{\omega}_{rJ}^a + (1/4)\sum_{i=1}^n H_{ii}(\zeta_r^a)^2\epsilon_i^2$. If $\bar{\phi}(\varrho_1) = (1/2)\sum_{J=1}^n\sum_{i=1}^n H_{iJ}\bar{\omega}_{ri}^a\bar{\omega}_{rJ}^a + (1/4)\sum_{i=1}^n H_{ii}(\zeta_r^a)^2\epsilon_i^2$, one gets $N(\bar{\phi}(\varrho_1)) = O(\sum_{i=1}^n|\bar{\omega}_{ri}^a|^3 + \sum_{i=1}^n|\eta_{ri}^a|^3+|\zeta_r^a|^3 + |\varepsilon|^3)$. From Lemma 2, one acquires $\varrho_2 = \bar{p}(\varrho_1) = \frac{1}{2}\sum_{J=1}^n\sum_{i=1}^n H_{iJ}\bar{\omega}_{ri}^a\bar{\omega}_{rJ}^a + (1/4)\sum_{i=1}^n H_{ii}(\zeta_r^a)^2\epsilon_i^2 + O(\sum_{i=1}^n|\bar{\omega}_{ri}^a|^3 + \sum_{i=1}^n|\eta_{ri}^a|^3+|\zeta_r^a|^3 + |\varepsilon|^3)$. According to Lemma 3, the "reduced" system can be obtained

$$\frac{d\bar{\omega}_r^a}{d\gamma} = -\vartheta\mu\varepsilon\check{K}\eta_r^a \tag{18}$$

$$\frac{d\eta_r^a}{d\gamma} = \vartheta\mu\varepsilon W^{-1}\left[\frac{\Xi\check{M}}{\Omega}\int_0^\Omega \upsilon(\bar{\omega}_r^a+\zeta_r^a Q(\varsigma))P(\varsigma)d\varsigma - \check{M}\eta_r^a\right] \tag{19}$$

$$\frac{d\tilde{\nu}_r^a}{d\gamma} = \vartheta\frac{\mu\check{\varpi}_H}{\Omega}\int_0^\Omega \upsilon(\bar{\omega}_r^a + \zeta_r^a Q(\varsigma))d\varsigma - \mu\check{\varpi}_H\tilde{\nu}_r^a \tag{20}$$

$$\frac{d\zeta_r^a}{d\gamma} = \lambda\vartheta\mu\varepsilon\check{\varpi}_C O\left(\sum_{i=1}^n|\bar{\omega}_{ri}^a|^3+\sum_{i=1}^n|\eta_{ri}^a|^3+|\zeta_r^a|^3+|\varepsilon|^3\right) - \vartheta\mu\varepsilon\check{\varpi}_C\zeta_r^a. \tag{21}$$

For (21), due to $\vartheta\mu\varepsilon\check{\varpi}_C > 0$, one has that (21) is locally exponentially stable at the origin. Next, we will consider the stability analysis of the systems (18)–(20). Let

$$\bar{\omega}_{ri}^{a,e} = \sum_{\kappa=1}^n b_\kappa^i\epsilon_\kappa + \sum_{h=1}^n\sum_{l=1}^n c_{hl}^i\epsilon_h\epsilon_l + O(|\epsilon|^3) \tag{22}$$

in which b_κ^i, c_{hl}^i are the real numbers. Furthermore, define

$$\upsilon(z) = \frac{1}{3!}\sum_{i=1}^n\sum_{J=1}^n\sum_{k=1}^n\frac{\partial^3\upsilon(0)}{\partial z_i\partial z_J\partial z_k}z_i z_J z_k + \frac{1}{2}\sum_{i=1}^n\sum_{J=1}^n\frac{\partial^2\upsilon(0)}{\partial z_i\partial z_J}z_i z_J + O(|z|^3). \tag{23}$$

From $(1/\Omega)\int_0^\Omega \sin^2\varpi_i t dt = (1/2)$, $(1/\Omega)\int_0^\Omega \sin^2\varpi_i t\sin^2\varpi_J t dt = (1/4)$, and $(1/\Omega)\int_0^\Omega \sin^4\varpi_i t dt = (3/8)$, one can further obtain

$$\begin{aligned}
0 &= \zeta_r^{a,e}\sum_{\substack{J=1\\J\neq p}}^n\frac{\partial^2\upsilon(0)}{\partial z_J\partial z_p}\left(\sum_{\kappa=1}^n b_\kappa^J\epsilon_\kappa + \sum_{h=1}^n\sum_{l=1}^n c_{hl}^J\epsilon_h\epsilon_l + O(|\epsilon|^3)\right) \\
&\quad + \zeta_r^{a,e}\left(\sum_{\kappa=1}^n b_\kappa^p\epsilon_\kappa + \sum_{h=1}^n\sum_{l=1}^n c_{hl}^p\epsilon_h\epsilon_l + O(|\epsilon|^3)\right) \\
&\quad \times\left(\sum_{\substack{J=1\\J\neq p}}^n\frac{\partial^3\upsilon(0)}{\partial z_J\partial^2 z_p}\left(\sum_{\kappa=1}^n b_\kappa^J\epsilon_\kappa + \sum_{h=1}^n\sum_{l=1}^n c_{hl}^J\epsilon_h\epsilon_l + O(|\epsilon|^3)\right)\right) \\
&\quad + \sum_{\substack{J=1\\J\neq p}}^n\frac{\partial^3\upsilon(0)}{\partial^2 z_J\partial z_p} \\
&\quad \times\left(\frac{1}{2}\zeta_r^{a,e}\left(\sum_{\kappa=1}^n b_\kappa^J\epsilon_\kappa + \sum_{h=1}^n\sum_{l=1}^n c_{hl}^J\epsilon_h\epsilon_l + O(|\epsilon|^3)\right)^2 + \frac{1}{4}(\zeta_r^{a,e})^3\epsilon_J^2\right) + \zeta_r^{a,e}\frac{1}{2}\sum_{\substack{J=1\\J\neq p}}^n\sum_{\substack{k=1\\k\neq p\\J\neq k}}^n\frac{\partial^3\upsilon(0)}{\partial z_J\partial z_k\partial z_p} \\
&\quad \times\left(\sum_{\kappa=1}^n b_\kappa^J\epsilon_\kappa + \sum_{h=1}^n\sum_{l=1}^n c_{hl}^J\epsilon_h\epsilon_l + O(|\epsilon|^3)\right) \\
&\quad \times\left(\sum_{\kappa=1}^n b_\kappa^k\epsilon_\kappa + O(|\epsilon|^3) + \sum_{h=1}^n\sum_{l=1}^n c_{hl}^k\epsilon_h\epsilon_l\right) \\
&\quad + \frac{\partial^3\upsilon}{\partial^3 z_p}(0) \\
&\quad \times\left(\frac{1}{2}\zeta_r^{a,e}\left(\sum_{\kappa=1}^n b_\kappa^p\epsilon_\kappa + \sum_{h=1}^n\sum_{l=1}^n c_{hl}^p\epsilon_h\epsilon_l + O(|\epsilon|^3)\right)^2 + \frac{1}{8}(\zeta_r^{a,e})^3\epsilon_p^2\right) + O(|\epsilon|^3).
\end{aligned}$$

Matching $\epsilon_\kappa, (\kappa = 1, \ldots, n)$ in the above-mentioned equation, one can obtain $[(\partial^2\upsilon(0))/(\partial z_1\partial z_p)b_1^1 + \cdots + (\partial^2\upsilon(0))/(\partial z_n\partial z_p)b_1^n]\epsilon_1 + \cdots + [(\partial^2\upsilon(0))/(\partial z_1\partial z_p)b_n^1 + \cdots + (\partial^2\upsilon(0))/(\partial z_n\partial z_p)b_n^n]\epsilon_n = 0$, for $p = 1, \ldots, n$. From $\epsilon_\kappa > 0$, one can derive $[(\partial^2\upsilon(0))/(\partial z_1\partial z_p), \cdots, .(\partial^2\upsilon(0))/(\partial z_n\partial z_p)]\Psi_\kappa = 0$ in which $\Psi_\kappa = [b_\kappa^1 \cdots b_\kappa^n]^T$. From (9), one can conclude that $b_\kappa^i = 0, (\kappa = 1, \cdots, n; i = 1, \cdots, n)$, due to $(\partial^2\upsilon(0))/(\partial z^2) = H$. Next, matching $\epsilon_h\epsilon_l, (h \neq l)$, one

can acquire $(c_{12}^1\epsilon_1\epsilon_2 + \cdots + c_{1n}^1\epsilon_1\epsilon_n + c_{21}^1\epsilon_2\epsilon_1 + \cdots + c_{nn-1}^1\epsilon_n\epsilon_{n-1})(\partial^2 \upsilon(0))/(\partial z_1\partial z_p) + \cdots + (c_{12}^n\epsilon_1\epsilon_2 + \cdots + c_{1n}^n\epsilon_1\epsilon_n + \cdots + c_{nn-1}^n\epsilon_n\epsilon_{n-1})(\partial^2 \upsilon(0))/(\partial z_n\partial z_p) = 0$, by further substituting $b_\kappa^i = 0$, for $p = 1, \ldots, n$. Since $\epsilon_h\epsilon_l > 0, (h \neq l)$, one can obtain $[(\partial^2 \upsilon(0))/(\partial z_1\partial z_p), \ldots, (\partial^2 \upsilon(0))/(\partial z_n\partial z_p)]\bar{\Psi}_{hl} = 0$ in which $\bar{\Psi}_{hl} = [c_{hl}^1, \ldots, c_{hl}^n]^T$. From (9), one has that $c_{hl}^i = 0, (i, h, l = 1, \ldots, n; h \neq l)$, due to $(\partial^2\upsilon(0))/(\partial z^2) = H$. Then, matching $\epsilon_h^2, (h = 1, \ldots, n)$, similarly, one has

$$\begin{bmatrix} c_{hh}^1 \\ \vdots \\ c_{hh}^h \\ \vdots \\ c_{hh}^n \end{bmatrix} = -\frac{1}{4}(e_r^{a,e})^3 \; H^{-1} \begin{bmatrix} \dfrac{\partial^3\upsilon(0)}{\partial z_h^2\partial z_1} \\ \vdots \\ \dfrac{1}{2}\dfrac{\partial^3\upsilon(0)}{\partial z_h^3} \\ \vdots \\ \dfrac{\partial^3\upsilon(0)}{\partial z_h^2\partial z_n} \end{bmatrix}, \quad h = 1, \ldots, n. \quad (24)$$

Thus, one can derive

$$\bar{\omega}_{ri}^{a,e} = \sum_{h=1}^{n} c_{hh}^i\epsilon_h^2 + O(|\epsilon|^3). \quad (25)$$

Moreover, according to (14) and (23), one has

$$\begin{aligned}\tilde{\nu}_r^{a,e} = {} & \frac{1}{2}\sum_{i=1}^{n}\sum_{j=1}^{n}\frac{\partial^2\,\upsilon(0)}{\partial z_i\partial z_j}\left(\bar{\omega}_{ri}^{a,e}\bar{\omega}_{rj}^{a,e} + \frac{1}{2}(\zeta_r^{a,e})^2\epsilon_i^2\right) \\ & + \frac{1}{3!}\sum_{i=1}^{n}\sum_{j=1}^{n}\sum_{k=1}^{n}\frac{\partial^3\,\upsilon(0)}{\partial z_i\partial z_j\partial z_k}\bar{\omega}_{ri}^{a,e}\bar{\omega}_{rj}^{a,e}\bar{\omega}_{rk}^{a,e} \\ & + \frac{1}{4}\frac{\partial^2\upsilon(0)}{\partial z_i\partial z_j^2}(\zeta_r^{a,e})^2\epsilon_j^2\bar{\omega}_{ri}^{a,e} + O(|\epsilon|^3). \quad (26)\end{aligned}$$

Substituting (25) into (26), one has $\tilde{\nu}_r^{a,e} = (1/4)(\zeta_r^{a,e})^2\sum_{i=1}^{n} H_{ii}\epsilon_i^2 + O(|\epsilon|^3)$. Thus, the Jacobian of (18)–(20) at $(\bar{\omega}_r^{a,e}, \eta_r^{a,e}, \tilde{\nu}_r^{a,e})$ can be obtained in the following:

$$J_a^r = \begin{bmatrix} A_{2n\times 2n} & B_{2n\times 1} \\ C_{1\times 2n} & D_{1\times 1} \end{bmatrix} \quad (27)$$

with

$$A = \begin{bmatrix} 0_{n\times n} & -\vartheta\,\mu\varepsilon\check{K}I \\ \vartheta\mu\varepsilon(I - \mu\varepsilon\vartheta\,\Xi\check{M}d)^{-1}\dfrac{\Xi\check{M}}{\Omega}\Pi & -\vartheta\,\mu\varepsilon(I - \mu\varepsilon\vartheta\,\Xi\check{M}d)^{-1}\check{M} \end{bmatrix} \quad (28)$$

$$\begin{aligned} C &= \left[\frac{\vartheta\,\mu\check{\varpi}_H}{\Omega}\int_0^{\Omega}\frac{\partial}{\partial\bar{\omega}}(\upsilon(\bar{\omega}_r^{a,e} + \zeta_r^{a,e}Q(\varsigma)))d\varsigma \;\; 0_{1\times n}\right] \\ B &= 0_{2n\times 1} \\ D &= -\vartheta\,\mu\check{\varpi}_H \end{aligned} \quad (29)$$

with $\Pi = \int_0^{\Omega}(\partial/\partial\bar{\omega})[\upsilon(\bar{\omega}_r^{a,e} + \zeta_r^{a,e}Q(\varsigma))P(\varsigma)]d\varsigma$. One has that $(1/\Omega)\int_0^{\Omega} P(\varsigma)(\partial/\partial\bar{\omega})\upsilon(\bar{\omega}_r^{a,e} + \zeta_r^{a,e}Q(\varsigma))d\varsigma = (1/\Omega)\int_0^{\Omega}\zeta_r^{a,e}Hd\varsigma + O(|\epsilon|)_{1\times n}$. Since $H > 0, \zeta_r^{a,e} > 0$, one can conclude that $A_{21} > 0$. Due to small positive constants μ, ε, and ϑ, J_r^a can be proven to be Hurwitz. Then, the origin of the systems (18)–(20) is asymptotically stable.

REFERENCES

[1] J. Popović-Gerber *et al.*, "Power electronics enabling efficient energy usage: Energy savings potential and technological challenges," *IEEE Trans. Power Electron.*, vol. 27, no. 5, pp. 2338–2353, May 2012.

[2] B. Sun, P. B. Luh, Q.-S. Jia, Z. Jiang, F. Wang, and C. Song, "Building energy management: Integrated control of active and passive heating, cooling, lighting, shading, and ventilation systems," *IEEE Trans. Autom. Sci. Eng.*, vol. 10, no. 3, pp. 588–602, Jul. 2013.

[3] M. A. Habib, M. Hasanuzzaman, M. Hosenuzzaman, A. Salman, and M. R. Mehadi, "Energy consumption, energy saving and emission reduction of a garment industrial building in Bangladesh," *Energy*, vol. 112, pp. 91–100, Oct. 2016.

[4] Y. Wang, A. Pandharipande, and P. Fuhrmann, "Energy data analytics for nonintrusive lighting asset monitoring and energy disaggregation," *IEEE Sensors J.*, vol. 18, no. 7, pp. 2934–2943, Apr. 2018.

[5] M. Amirkhani, V. Garcia-Hansen, G. Isoardi, and A. Allan, "Innovative window design strategy to reduce negative lighting interventions in office buildings," *Energy Buildings*, vol. 179, pp. 253–263, Nov. 2018.

[6] C. Yin *et al.*, "Design of optimal lighting control strategy based on multi-variable fractional-order extremum seeking method," *Inf. Sci.*, vol. 465, pp. 38–60, Oct. 2018.

[7] *Office of Energy Efficiency and Renewable Energy*, U.S. Dept. Energy, Washington, DC, USA, 2011.

[8] T.-J. Park and S.-H. Hong, "Experimental case study of a BACnet-based lighting control system," *IEEE Trans. Autom. Sci. Eng.*, vol. 6, no. 2, pp. 322–333, Apr. 2009.

[9] D. Tran and Y. K. Tan, "Sensorless illumination control of a networked led-lighting system using feedforward neural network," *IEEE Trans. Ind. Electron.*, vol. 61, no. 4, pp. 2113–2121, Apr. 2014.

[10] D. Caicedo and A. Pandharipande, "Sensor-driven lighting control with illumination and dimming constraints," *IEEE Sensors J.*, vol. 15, no. 9, pp. 5169–5176, Sep. 2015.

[11] G. Shahzad, H. Yang, A. W. Ahmad, and C. Lee, "Energy-efficient intelligent street lighting system using traffic-adaptive control," *IEEE Sensors J.*, vol. 16, no. 13, pp. 5397–5405, Jul. 2016.

[12] Q. Yao, L. Yuan, and Y. Bian, "Establishment of vision effect diagram for optimization of smart LED lighting," *IEEE Photon. J.*, vol. 8, no. 4, Aug. 2016, Art. no. 1601508.

[13] M. Mayhoub and D. Carter, "A feasibility study for hybrid lighting systems," *Building Environ.*, vol. 53, pp. 83–94, Jul. 2012.

[14] K. B. Ariyur and M. Krstić, *Real-Time Optimization by Extremum-Seeking Control*. Hoboken, NJ, USA: Wiley, 2003.

[15] Y. Tan, D. Nešić, and I. Mareels, "On non-local stability properties of extremum seeking control," *Automatica*, vol. 42, pp. 889–903, Jun. 2006.

[16] C. Yin, Y. Q. Chen, and S.-M. Zhong, "Fractional-order sliding mode based extremum seeking control of a class of nonlinear systems," *Automatica*, vol. 50, no. 12, pp. 3173–3181, 2014.

[17] L. Wang, S. Chen, and K. Ma, "On stability and application of extremum seeking control without steady-state oscillation," *Automatica*, vol. 68, pp. 18–26, Jun. 2016.

[18] S. Dadras, "Path tracking using fractional order extremum seeking controller for autonomous ground vehicle," SAE Tech. Paper 2017-01-0094, 2017.

[19] B. Calli, W. Caarls, M. Wisse, and P. P. Jonker, "Active vision via extremum seeking for robots in unstructured environments: Applications in object recognition and manipulation," *IEEE Trans. Autom. Sci. Eng.*, vol. 15, no. 4, pp. 1810–1822, Oct. 2018.

[20] T. T. Ashley and S. B. Andersson, "Tracking a diffusing three-dimensional source via nonholonomic extremum seeking," *IEEE Trans. Autom. Control*, vol. 63, no. 9, pp. 2855–2866, Sep. 2018.

[21] C. Yin, B. Stark, Y. Q. Chen, and S.-M. Zhong, "Adaptive minimum energy cognitive lighting control: Integer order vs fractional order strategies in sliding mode based extremum seeking," *Mechatronics*, vol. 23, pp. 863–872, Oct. 2013.

[22] C. Yin, B. Stark, Y. Q. Chen, S.-M. Zhong, and E. Lau, "Fractional-order adaptive minimum energy cognitive lighting control strategy for the hybrid lighting system," *Energy Buildings*, vol. 87, pp. 176–184, Jan. 2015.

[23] A. Ghaffari, M. Krstić, and D. Nešić, "Multivariable Newton-based extremum seeking," *Automatica*, vol. 48, pp. 1759–1767, Aug. 2012.

[24] S.-J. Liu and M. Krstic, "Newton-based stochastic extremum seeking," *Automatica*, vol. 50, pp. 952–961, Mar. 2014.

[25] T. R. Oliveira, M. Krstić, and D. Tsubakino, "Extremum seeking for static maps with delays," *IEEE Trans. Autom. Control*, vol. 62, no. 4, pp. 1911–1926, Apr. 2017.

[26] C. Yin, S. Wu, S. Zhou, J. Cao, X. Huang, and Y. Cheng, "Design and stability analysis of multivariate extremum seeking with Newton method," *J. Franklin Inst.*, vol. 355, no. 4, pp. 1559–1578, 2018.
[27] C. Yin, S. Dadras, X. Huang, J. Mei, H. Malek, and Y. Cheng, "Energy-saving control strategy for lighting system based on multivariate extremum seeking with Newton algorithm," *Energy Convers. Manage.*, vol. 142, pp. 504–522, Jun. 2017.
[28] C. Yin, S. Dadras, X. Huang, H. Malek, and Y. Cheng, "Optimal lighting control strategy for lighting system based on multivariable fractional-order extremum seeking method," in *Proc. Annu. Amer. Control Conf. (ACC)*, Jun. 2018, pp. 3098–3103.
[29] S. S. Yoon, J. S. Min, and J. S. Chun, "Effects of the deposition temperature on the resistivity of copper films produced by low-pressure metal-organic chemical vapour deposition on a TiN barrier layer," *J. Mater. Sci.*, vol. 30, no. 8, pp. 2029–2034, 1995.
[30] W. Steinhögl, G. Schindler, G. Steinlesberger, and M. Engelhardt, "Size-dependent resistivity of metallic wires in the mesoscopic range," *Phys. Rev. B, Condens. Matter*, vol. 66 no. 7, 2002, Art. no. 075414.
[31] W. Zhang, S. H. Brongersma, Z. Li, D. Li, O. Richard, and K. Maex, "Analysis of the size effect in electroplated fine copper wires and a realistic assessment to model copper resistivity," *J. Appl. Phys.*, vol. 101, no. 6, 2007, Art. no. 063703.
[32] F. Moisy *et al.*, "Influence of intermetallic compounds on the electrical resistivity of architectured copper clad aluminum composites elaborated by a restacking drawing method," *Mater. Des.*, vol. 155, pp. 366–374, Oct. 2018.
[33] J. Carr, *Applications of Centre Manifold Theory*. New York, NY, USA: Springer-Verlag, 1981.

Chun Yin (M'14) received the Ph.D. degree from the School of Mathematics Science, University of Electronic Science and Technology of China, Chengdu, China, in 2014.

From 2011 to 2012, she was an exchange Ph.D. student with the Center for Self-Organizing and Intelligent Systems, Department of Electrical Engineering, Utah State University, Logan, UT, USA. From 2012 to 2013, she was an exchange Ph.D. student with the MESA Laboratory, University of California at Merced, Merced, CA, USA. Since July 2014, she has been an Associate Professor with the School of Automation Engineering, University of Electronic Science and Technology of China. Her research interests include optimal control, extremum seeking control, stability analysis, and cognitive control.

Sara Dadras (SM'18) received the B.Sc. degree in electrical engineering from Shiraz University, Shiraz, Iran, in 2006, and the M.Sc. and Ph.D. degrees in electrical engineering from Tarbiat Modares University, Tehran, Iran, in 2008 and 2012, respectively.

In 2012, she joined the Electrical and Computer Engineering Department, Utah State University, Logan, UT, USA, as a Research Fellow. Her current research interests include hybrid electric vehicles, autonomous vehicles, renewable energy systems, nonlinear systems and control, and applied fractional calculus in controls.

Dr. Dadras is a member of ASME and SAE. She serves as an Associate Editor the for IEEE TRANSACTIONS ON AUTOMATION SCIENCE AND ENGINEERING and the *Asian Journal of Control*. She is the Organizer for the SAE Electronics Technical Committee.

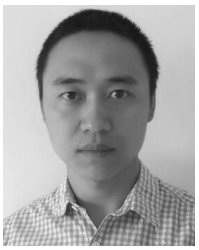

Xuegang Huang was born in 1985. He received the B.S. degree in materials science and engineering from the University of Southwest Jiaotong University, Chengdu, China, in 2008, and the M.S. and Ph.D. degrees from the Mechanical Engineering College, Shijiazhuang, China, in 2010 and 2014, respectively.

He is currently with the Hypervelocity Aerodynamic Institute, China Aerodynamics Research and Development Center, Mianyang, China, where he is an Associate Researcher. His doctoral dissertation was selected as the National Excellent Doctoral Dissertation of China in 2017. His research interests are in spacecraft measurement and control technology, space shielding engineering, hypervelocity impact engineering, and material dynamic behavior.

YangQuan Chen (SM'98) received the Ph.D. degree from Nanyang Technological University, Singapore, in 1998.

From 2000 to 2012, he was on the Faculty of Electrical Engineering with Utah State University, Logan, UT, USA. In 2012, he joined the School of Engineering, University of California at Merced, Merced, CA, USA, where he teaches mechatronics, engineering service learning, and unmanned aerial systems for undergraduates and fractional order mechanics and nonlinear controls for graduates. His current research interests include mechatronics for sustainability, cognitive process control, small multi-UAV-based cooperative multispectral personal remote sensing and applications, applied fractional calculus in controls, modeling, and signal processing, and distributed measurement and distributed control of distributed parameter systems using mobile actuator and sensor networks.

Dr. Chen is a member of the IEEE-USA's Committee on Transportation and Aerospace Policy. He serves as the Steering Committee Chair for the International Conference on Fractional Derivatives and Applications, and a Program Chair for 2016 International Conference on Unmanned Aircraft Systems. He is currently the Topic Editor-in-Chief of the *International Journal of Advanced Robotic Systems* (Field Robotics) and a Senior Editor of the *International Journal of Intelligent Robotic Systems*. He is an Associate Editor of *Fractional Calculus and Applied Analysis*, the IEEE TRANSACTIONS ON CONTROL SYSTEMS TECHNOLOGY, *Mechatronics*, *Control Engineering Practice*, *IET Control Theory and Applications*, and *ISA Transactions*.

Shouming Zhong was born on November 5, 1955. He received the B.S. degree in applied mathematics on differential equation from the University of Electronic Science and Technology of China, Chengdu, China, in 1981.

Since June 1997, he has been a Professor with the School of Mathematical Sciences, University of Electronic Science and Technology of China. His research interests are stability theorem and its application research of the nonlinear system, the robustness control, neural network, and nonlinear control.

Mr. Zhong is the Director of the Chinese Mathematical Biology Society and the Chair of Biomathematics in Sichuan. He is the Editor of the *Journal of Biomathematics*.